Environ Sci Pollut Res (2017) 24:24235–24242
DOI 10.1007/s11356-017-0036-9

RESEARCH ARTICLE

Effective adsorbent for arsenic removal: core/shell structural nano zero-valent iron/manganese oxide

Trung Huu Bui[1] · **Choonsoo Kim**[1] · **Sung Pil Hong**[1] · **Jeyong Yoon**[1,2]

Received: 11 April 2017 / Accepted: 25 August 2017 / Published online: 9 September 2017

Abstract Recently, nano zero-valent iron (nZVI) has emerged as an effective adsorbent for the removal of arsenic from aqueous solutions. However, its use in various applications has suffered from reactivity loss resulting in a decreased efficiency. Thus, the aim of this study was to develop an effective arsenic adsorbent as a core/shell structural nZVI/manganese oxide (or nZVI/Mn oxide) to minimize the reactivity loss of the nZVI. As the major result, the arsenic adsorption capacities of the nZVI/Mn oxide for As(V) and As(III) were approximately two and three times higher than that of the nZVI, respectively. In addition, the As(V) removal efficiency of the nZVI/Mn oxide was maintained through 4 cycles of regeneration whereas that of the nZVI was decreased significantly. The enhanced reactivity and reusability of the nZVI/Mn oxide can be successfully explained by the synergistic interaction of the nZVI core and manganese oxide shell, in which the manganese oxides participate in oxidation reactions with corroded Fe^{2+} and subsequently retard the release of aqueous iron providing additional surface sites for arsenic adsorption. In summary, this study reports the successful fabrication of a core/shell nZVI/Mn oxide as an effective adsorbent for the removal of arsenic from aqueous solutions.

Keywords Arsenic removal · Nano zero-valent iron · Manganese oxide · Core/shell structure · Adsorption

Responsible editor: Guilherme L. Dotto

Electronic supplementary material The online version of this article (https://doi.org/10.1007/s11356-017-0036-9) contains supplementary material, which is available to authorized users.

✉ Jeyong Yoon
jeyong@snu.ac.kr

[1] School of Chemical and Biological Engineering, College of Engineering, Institute of Chemical Process, Seoul National University (SNU), Gwanak-gu, Daehak-dong, Seoul 151-742, Republic of Korea

[2] Asian Institute for Energy, Environment & Sustainability (AIEES), Seoul National University (SNU), Gwanak-gu, Daehak-dong, Seoul 151-742, Republic of Korea

Introduction

Arsenic (As) is a well-known dangerous and carcinogenic chemical with adverse effects on humans, animals, and other living organisms (Bang et al. 2005b; Choong et al. 2007; Mohan and Pittman 2007). Many efforts have focused on reducing the arsenic level in drinking water for safe consumption. Most of the arsenic removal technologies are classified into four processes: membrane filtration (including RO), coagulation–filtration precipitation (including lime softening), ion exchange, and adsorption. Among them, adsorption technologies have been commonly used due to their simplicity, effectiveness, and low cost (Singh et al. 2015; Xu et al. 2002). Various kinds of adsorbents have been used including metal oxides (Chang et al. 2009; Hristovski et al. 2007; Mayo et al. 2007), polymeric resins (Korngold et al. 2001; Rivas et al. 2007; Zhang et al. 2008), activated carbon (Asadullah et al. 2014; Yang et al. 2007), and hybrid materials (Gupta et al. 2009; Ramesh et al. 2007; Sarkar et al. 2007).

Recently, nano zero-valent iron (nZVI) was reported as one of the effective adsorbents for the removal of arsenic (As(III) and As(V)). The outstanding arsenic adsorption property of nZVI is explained by the role of its reactive corroded products (Fe species) in both the adsorption and co-precipitation processes (Fu et al. 2014; Kanel et al. 2005; Tanboonchuy et al. 2011). Despite its effectiveness in arsenic removal, a decrease in the adsorption efficiency of nZVI is explained by the formation of iron (hydr)oxides on the nZVI surface, which has

commonly been reported as reactivity loss or efficiency loss (Btatkeu-K et al. 2014a; Noubactep 2010; Noubactep et al. 2011; Sato 1989). Consequently, fixed-bed applications of nZVI systems have suffered from accumulation and rapid clogging of its by-products as well as from difficulties in regeneration (Tang and Lo 2013).

Several approaches have been tried to sustain the reactivity of zero-valent iron including bimetallic Fe^0/Me^0 systems (Bokare et al. 2008; Ghauch et al. 2010a) and admixing Fe^0 with other materials (Noubactep et al. 2012). The bimetallic composite of Fe^0 with a more noble metal (such as Ni, Cu, and Pd) was done to promote the Fe^0 corrosion rate, which showed some extent of success for the degradation of organic substances (Bokare et al. 2008; Ghauch et al. 2010a). However, the expansive nature of the corrosion products (iron (hydr)oxides) from these systems was still a problem causing rapid clogging in a column filtration system (Noubactep et al. 2012). Unlike inert materials, MnO_2 particles with a porous structure were recently introduced as a reactive mineral for sustaining the reactivity of Fe^0, which were used in the removal of contaminated methylene blue (Btatkeu-K et al. 2014a) and clofibric acid (Ghauch et al. 2010b). The extended reactivity of Fe^0 in the admixing system with MnO_2 was explained by the fact that the Fe^{2+} (corroded from Fe^0) could be transported to and reacted with the MnO_2 particles (Btatkeu-K et al. 2014a). These oxidation reactions occurring near porous MnO_2 particles contribute to avoiding or delaying the precipitation of the oxide film on the Fe^0 surface and thus maintaining the efficiency of the Fe^0 system. However, the volume fraction of the Fe^0 in the filtration column was only about 25% (Btatkeu-K et al. 2014b), which was in addition to the low mechanical strength of the MnO_2. Therefore, a new extensive design is required for a system to achieve the desirable performance. Moreover, the application of these approaches for arsenic removal remains an unexplored area.

This study reports the development of a core/shell structural nano zero-valent iron/manganese oxide (called nZVI/Mn oxide) adsorbent for better performance in arsenic removal compared with that of nZVI.

Experiments

Materials and chemicals

All chemicals including the nZVI (35 ~ 45 nm) used in this study were of analytical and synthetic grades purchased from Sigma-Aldrich. The As(III) and As(V) stock solutions (1000 mg L^{-1}) were prepared in deionized (DI) water using $NaAsO_2$ and $NaHAsO_4{\cdot}7H_2O$ salts, respectively. The arsenic working solution was freshly diluted from these stock solutions by DI water prior to its use.

Preparation of the nZVI/Mn oxide

The nZVI/Mn oxide was synthesized with a simple procedure using a sonochemical synthesis (Dharmarathna et al. 2012; Kawaoka et al. 2005) as follows. A suspended solution, in which the nZVI was added to a 0.2 M $KMnO_4$ solution and adjusted to pH 1 with HCl, was sonicated at room temperature for 30 min (a Sonics Vibra-Cell VCX-500 Ultrasonic Processor). The dark ground precipitate was aged for 2 h. Finally, a solid powder collected from centrifuging was washed many times with DI water and acetone and dried in a vacuum at 70 °C.

Analytical methods

The arsenic concentration was analyzed with an inductively coupled plasma–atomic emission spectrometer (ICP-AES, ICPS-7500, Shimadzu, Japan). Other concentrations of metals were measured with an ICP-AES and UV/Vis spectrometer (8453E UV/Vis, Agilent, USA). The morphology and surface characterization of the nZVI/Mn oxide and the nZVI were analyzed with a scanning electron microscope (SEM, JSM-6700F, Jeol, Japan), high-resolution transmission electron microscope (HR-TEM, JEM 3010, Jeol, Japan), high-resolution X-ray diffractometer (XRD, D8 Discover, Bruker, Germany), and X-ray photoelectron spectroscope (XPS, Sigma Probe, ThermoVG, UK). The specific surface area and pore volume of the materials were measured with a BET analyzer (ASAP 2000, Micromeritics, USA), while their zeta potentials were evaluated with an electrophoretic light-scattering spectrophotometer (ELS-8000, Otsuka, Japan).

Batch adsorption experiments

Batch adsorption experiments for the removal of both As(III) and As(V) with either the nZVI/Mn oxide (0.3 g L^{-1}) or the nZVI for comparison were typically done at a pH of 4.8 and 25 °C for 120 min in glass shaking bottles (100 mL bottles shook at 200 rpm), and an arsenic concentration (As(III) or As(V)) of 5 mg L^{-1} was used. An equilibration time of 120 min was selected after a kinetic study (see in Supporting information). The solutions sampled at the predetermined time were centrifuged for 10 min (4000 rpm), and the supernatant solutions were used for the arsenic analysis.

For the kinetic study, 5 mL of the adsorption solution was withdrawn at predetermined times up to 150 min from 200 mL of the arsenic solution (5 mg L^{-1}) containing 0.3 g L^{-1} nZVI/Mn oxide adsorbent (refer to Fig. S1 in the SI for the details). An adsorption isotherm was done by varying the initial concentration of arsenic from 1 to 20 mg L^{-1}, while the adsorbent dose of 0.3 g L^{-1} was maintained. Note that the equilibrium test was conducted for 120 min for both adsorptions of As(III)

Table 1 Characteristics of the core/shell nZVI/Mn oxide compared with the nZVI

Contents	nZVI/Mn oxide	nZVI
BET surface area ($m^2\ g^{-1}$)	16.0	11.8
Pore volume ($cm^3\ g^{-1}$)	0.100	0.053
Zeta potential (ζ mV)[a]	− 27.6	− 12.6
Particle size (nm)	35–45	35–45
Thickness of Mn oxide shell (nm)	~ 5 nm (amorphous structure)	–
Manganese oxidation states	+ 2, + 3, or + 4	–
Mn wt%	4.5%	–

[a] Zeta potential was measured at pH 7

and As(V) due to their fast kinetic adsorption (see Fig. S1 in the SI).

The effect of pH on the adsorption of arsenic by the nZVI/Mn oxide compared with the nZVI was examined at a pH range from 3 to 11. The pH during the adsorption process was maintained at the initial pH value by adding HCl or NaOH solution every 15 min. H_2SO_4 was not chosen because sulfate oxyanion could be competitive for adsorption with As(V) or As(III), especially at low pH (Su and Puls 2001b; Zhu et al. 2009), causing the unnecessary complexity.

The regeneration test of the nZVI/Mn oxide adsorbent was done with four successive cycles of adsorption–desorption and compared with the nZVI to evaluate their loss of reactivity. The regeneration experiment was done by shaking the arsenic-laden adsorbents in 0.1 M NaOH (15 mL) for 2 h at 200 rpm. All the supernatants obtained during the four successive cycles of the adsorption–desorption were analyzed for iron and arsenic concentrations to examine the reusability of the nZVI/Mn oxide including the amount of iron released compared with the nZVI.

Results

Characterization of the nZVI/Mn oxide

Table 1 shows the characteristics of the core/shell nZVI/Mn oxide compared with the nZVI. As shown in Table 1, both the surface area (BET) and pore volume of the nZVI/Mn oxide are 36 and 87% larger than that of the nZVI, respectively. For example, the surface area and pore volume of the nZVI/Mn oxide increased from 11.8 to 16.0 $m^2\ g^{-1}$ and from 0.053 to 0.100 $cm^3\ g^{-1}$ relative to nZVI, respectively, while the Mn weight percent in the case of the nZVI/Mn oxide was around 4.5%.

Figure 1 shows the surface characteristics of the nZVI/Mn oxide compared with the nZVI examined by HR-TEM images (Fig. 1a), SEM images (Fig. 1b), XRD patterns (Fig. 1c), and XPS patterns (Mn 2*p* and Fe 2*p*) (Fig. 1d). As seen in Fig. 1a, b, the nZVI/Mn oxide and nZVI particles appear to be spherical with a size of ~ 40 nm. In particular, the TEM image of the nZVI/Mn oxide clearly shows the core/shell structure with an additional manganese oxide layer (~ 5 nm) covering the iron oxide layer on the nZVI, whereas the image of the nZVI shows only the iron oxide layer on the Fe^0 core. The XRD pattern of the nZVI/Mn oxide (Fig. 1c) appears to be very similar with that of the nZVI with two sharp peaks for the predominant Fe^0 (2θ = 44.7° and 65.0°) suggesting that the Fe^0 structure was placed inside of the nZVI/Mn oxide adsorbent (Kanel et al. 2005; Sun et al. 2006). Additionally, iron oxides and manganese oxides were presumed to be amorphous because no obvious relevant crystalline peaks were detected (Wen et al. 2014; Xi et al. 2010; Zhao et al. 2012). Figure 1d clearly shows the specific XPS peaks for Fe^{3+} and Fe^{2+} for both the nZVI/Mn oxide and nZVI. It is interesting to observe that Fe^0 (Fe 2*p*), which was located at 706.5 eV in the spectrum for nZVI, disappeared in the spectrum for the nZVI/Mn oxide possibly due to the shielding effect of the outer layers of the iron oxide and manganese oxide which was shown in Fig. 1a (Grosvenor et al. 2004; Wang et al. 2014; Yamashita and Hayes 2008). On the other hand, specific XPS peaks (Mn 2*p*) of the nZVI/Mn oxide were observed showing several manganese oxidation states (+ 2, + 3, or + 4) (Ahn et al. 2014; Nesbitt and Banerjee 1998; Shan and Tong 2013). All the results in Fig. 1 show the successful fabrication of the core/shell structure of the nZVI/Mn oxide.

Enhanced arsenic removal of the nZVI/Mn oxide

Figure 2a shows the pH effect on the arsenic adsorption capacity of the nZVI/Mn oxide compared with that of the nZVI as the pH was varied from 3 to 11. As shown in Fig. 2a, the general tendency of the As (III) and As (V) adsorptions for the nZVI/Mn oxide was quite similar to that for the nZVI but exhibited a better removal in an acidic solution. For example, at pH 4, the adsorption capacities were 16.4 and 10.5 mg g^{-1} for As(V) adsorption on the nZVI/Mn oxide and the nZVI, respectively, while those significantly dropped at high pH conditions (> pH 5) for both cases. The pH dependence was well consistent with previous studies on nZVI (Bang et al. 2005b; Su and Puls 2001a). One explanation for the strong pH dependence in the low-pH region is that the oxidation (corrosion) of Fe^0 promoted in acidic conditions (pH < 5) provides fresh adsorption sites as iron (hydr)oxide products ($Fe(OH)_2$, $Fe(OH)_3$ and Fe_3O_4) for the adsorption and co-precipitation of arsenic (Tanboonchuy et al. 2011). In the case of the high-pH conditions, the weak interaction between the

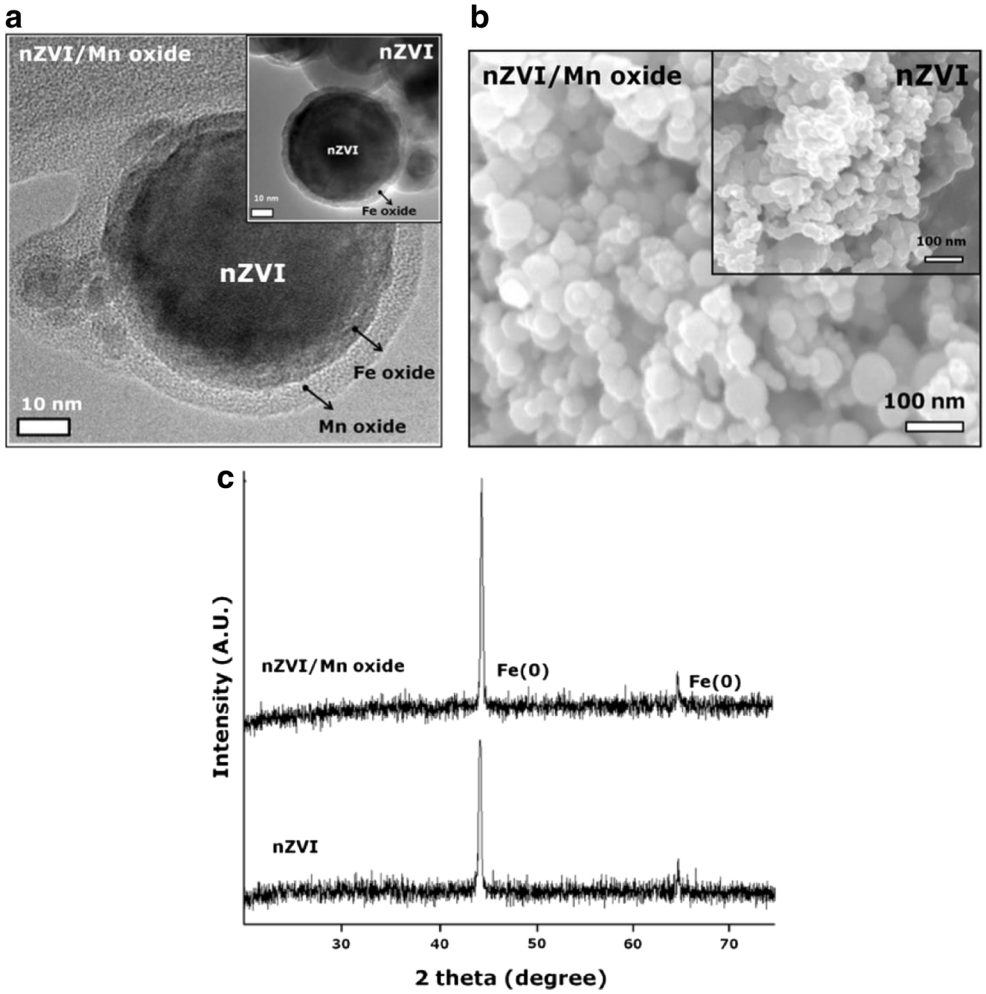

Fig. 1 Surface characteristics of the nZVI/Mn oxide compared with the nZVI examined by HR-TEM images (**a**), SEM images (**b**), XRD patterns (**c**), and XPS patterns (Fe 2*p* and Mn 2*p*) (**d**)

As(V) species and the adsorbent due to the low corrosion rate of Fe^0 (nZVI) as well as their negative columbic repulsion (Su and Puls 2001a; Tanboonchuy et al. 2011) contributed to the low adsorption capacity of the nZVI/Mn oxide and the nZVI. On the other hand, both adsorbents exhibited less pH dependence for As(III) adsorption due to its neutral form (pH < 9) than that of the As(V) adsorption.

Figure 2b shows the As(III) and As(V) adsorption isotherms of the nZVI/Mn oxide with the fitting of the Langmuir isotherm model (pH 4.8) compared with the nZVI. As shown in Fig. 2, the adsorption isotherms for both the nZVI/Mn oxide and nZVI were well-fitted with the Langmuir isotherm model ($R^2 \geq 0.99$ for all) (Bhowmick et al. 2014; Wang et al. 2014; Zhu et al. 2009) indicating the monolayer adsorption of As(III) or As(V) on the nZVI/Mn oxide and nZVI. The maximum arsenic adsorption capacities (q_m) calculated for the nZVI/Mn oxide (29.4 mg g^{-1} for As(III) and 35.7 mg g^{-1} for As(V)) were significantly larger than the values obtained for the nZVI (9.5 mg g^{-1} for As(III) and 21.7 mg g^{-1} for As(V)).

Enhanced reusability of the nZVI/Mn oxide

Figure 3a, b shows the results of the arsenic removal (As(III) and As(V)) and the released concentration of iron up to 4 cycles of regeneration. As shown in Fig. 3a, the arsenic removal of the nZVI/Mn oxide up to the 4th cycle of adsorption/desorption was much better than that of the nZVI. Especially for As(V) adsorption, the nZVI/Mn oxide exhibited approximately 100% removal for each adsorption experiment in the regeneration test, whereas the removal performance for the nZVI gradually decreased to below 70% at the 4th cycle. In the case of As(III), although the performance of the nZVI/Mn oxide was not as good as that of As(V), the As(III) removal of the nZVI/Mn oxide was still better than that of the nZVI in the first 2 cycles of the adsorption.

Figure 3b shows that a much lower iron concentration was released from the nZVI/Mn oxide than from the nZVI for both As(III) and As(V). For example, the iron concentration released from the nZVI ranged from 4 to 9 mg L^{-1} for the As(III) adsorption and from 5 to 31 mg L^{-1} for the As(V) adsorption,

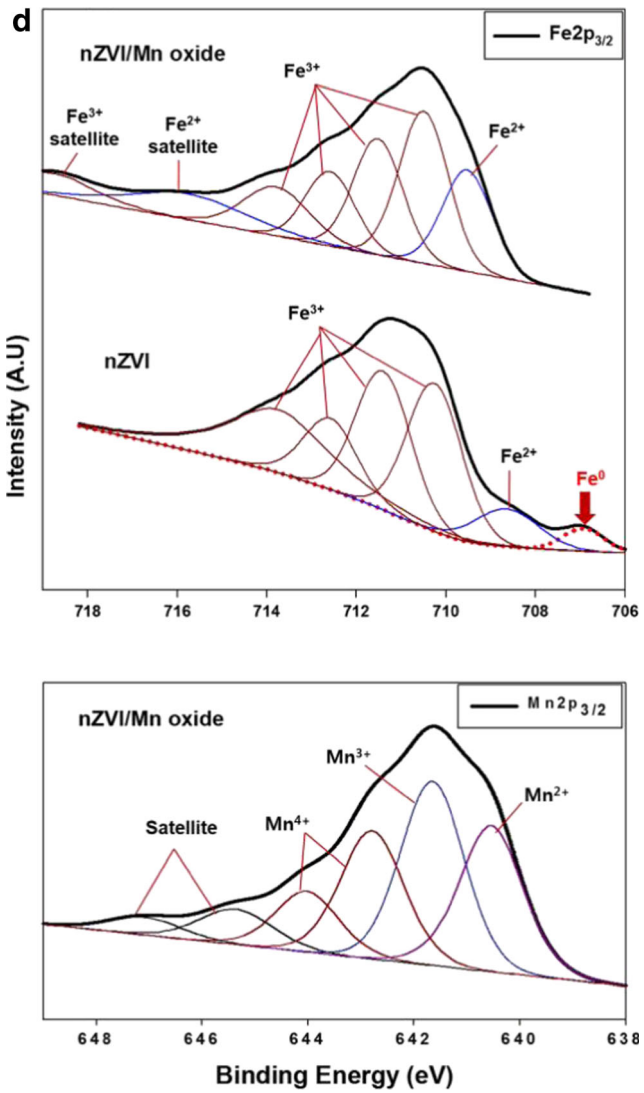

Fig. 1 continued.

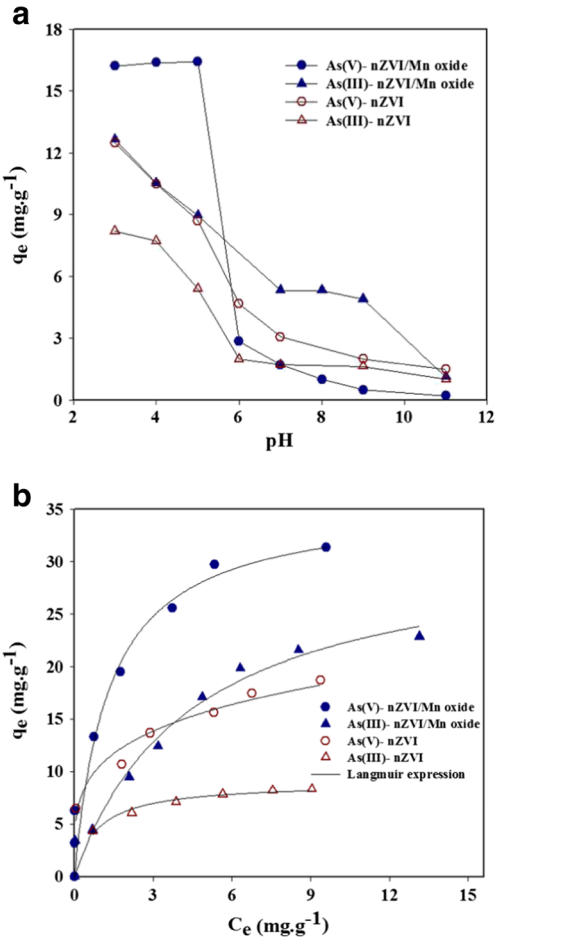

Fig. 2 Comparison of **a** adsorption capacity between the nZVI/Mn oxide and the nZVI for As(III) and As(V) with respect to pH and **b** adsorption isotherms between the nZVI/Mn oxide and the nZVI for As(III) and As(V) (adsorbent dose = 0.3 g L^{-1}, pH = 4.8 ~ 4.9, 25 °C)

while the iron concentration released from the nZVI/Mn oxide was insignificant for the As(III) and As(V) adsorptions. Note that the lower release of iron from the nZVI for the As(III) adsorption compared with that for the As(V) adsorption in Fig.3b was consistent with the literature (Bang et al. 2005a).

Discussion

The reaction activity of the nZVI adsorbent can be explained by a series of chemical reactions on the surface of the nZVI (Eqs. (1)–(7)) reported in the literature (Fu et al. 2014; Kanel et al. 2005; Tanboonchuy et al. 2011). As shown in Eqs. (1)–(3), the corrosion process of nZVI is stimulated in acidic condition subsequently producing Fe^{2+} which can be further oxidized to the Fe^{3+} form. These corrosion products (Fe^{2+} and Fe^{3+}) can further provide fresh adsorption or precipitation sites as iron (hydr)oxide products ($Fe(OH)_2$, $Fe(OH)_3$ and Fe_3O_4) on nZVI surface (Eqs. (5)–(7)). In addition, the oxidation species $^{\cdot}OH$ (Eq. (3)) can oxidize As(III) to As(V) to enhance the As(III) adsorption (Eq. (4)). However, the difficulty of corrosion occurring in the nZVI at the high-pH region leads to a reduced adsorption performance of the nZVI, which is consistent with the results in Fig. 2a.

$$Fe_s^0(nZVI) + O_2 + 2H^+ \rightarrow Fe^{2+} + H_2O_2 \quad (1)$$

$$Fe_s^0(nZVI) + H_2O_2 + 2H^+ \rightarrow Fe^{2+} + 2H_2O \quad (2)$$

$$Fe^{2+} + H_2O_2 \rightarrow Fe^{3+} + {}^{\cdot}OH + OH^- \quad (3)$$

$$As(III) + {}^{\cdot}OH + H^+ \rightarrow As(V) + H_2O \quad (4)$$

$$Fe^{2+} + 2OH^- \rightarrow Fe(OH)_2 \quad (5)$$

$$Fe^{3+} + 3OH^- \rightarrow Fe(OH)_3 \quad (6)$$

$$6Fe(OH)_2 + O_2 \rightarrow 2Fe_3O_4 + 6H_2O \quad (7)$$

Figure 4 shows the Mn 2*p* XPS spectra of the nZVI/Mn oxide before and after arsenic adsorption. As shown in Fig. 4,

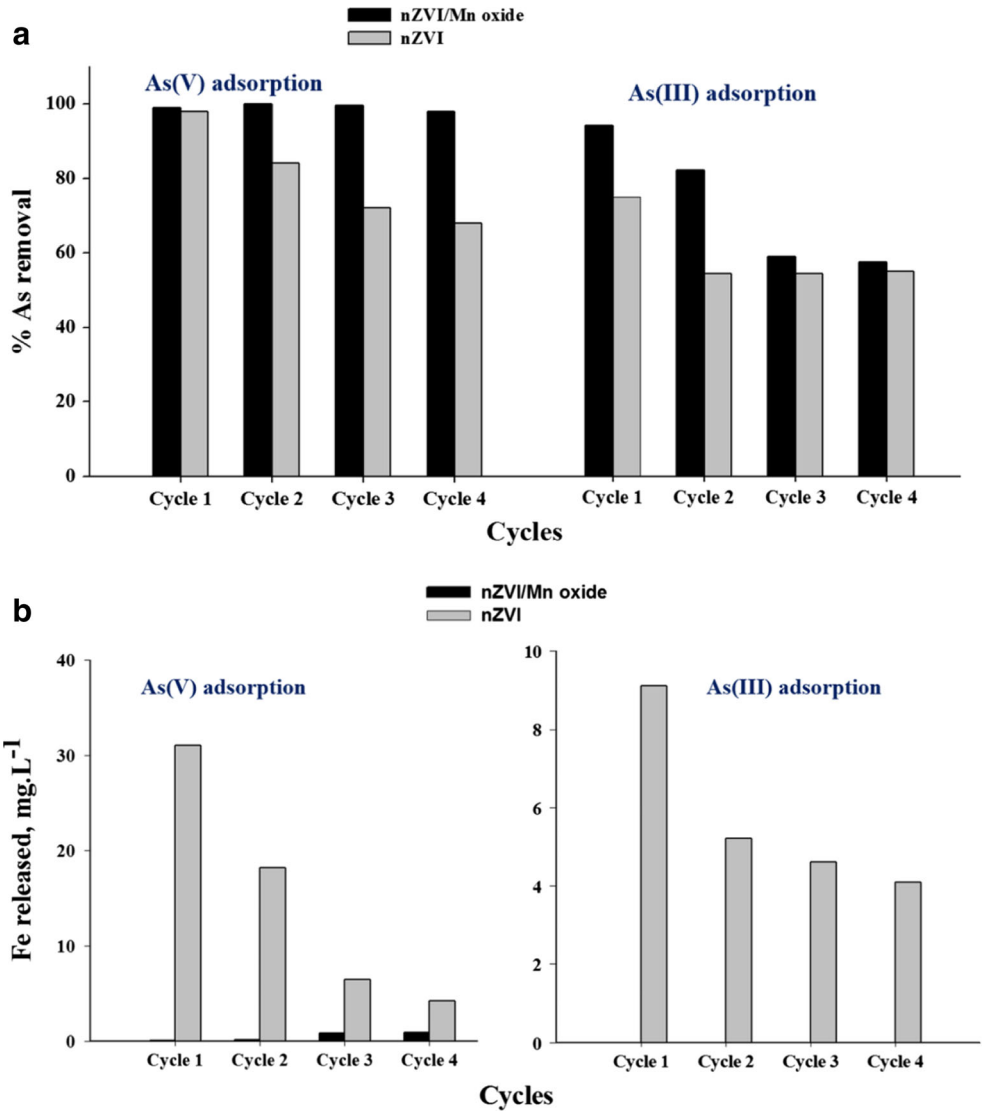

Fig. 3 Comparison of the arsenic removal between the nZVI/Mn oxide and the nZVI (**a**) and iron concentrations released (**b**) after As(III) and As(V) adsorptions for each cycle of regeneration, respectively ($[As(III)]_0 = [As(V)]_0 = 2$ mg L^{-1}, pH = 4.8 ~ 4.9, adsorbent dose = 0.6 g L^{-1}, regenerant solution: 0.25 mL of 0.1 M NaOH for 1 mg of adsorbent, 2 h for desorption and adsorption)

the Mn 2*p* peak of the pristine nZVI/Mn oxide was negatively shifted to the low-binding-energy side not only after the As(III) sorption but also after the As(V) sorption (Btatkeu-K et al. 2014a; Noubactep et al. 2011) indicating that a fraction of Mn species in the manganese oxide layer was reduced to lower oxidation states (Wu et al. 2012).

Considering the common structure of the nZVI/Mn oxide adsorbent with nZVI which is the core nZVI covered with Fe oxide (Fig. 1a, b) and the similar pH-dependent behavior (Fig. 2a), the reaction activity of the nZVI/Mn oxide adsorbent can be similarly explained with the chemistry of nZVI as shown in Eqs. (1)–(7). Then, recognizing Eqs. (1)–(7) in the behavior of the nZVI/Mn oxide adsorbent, the reduction of Mn species in the shell is explained by the reactions of manganese oxide with the corroded Fe^{2+} from the nZVI (Eqs. (8) and (9)).

$$Fe^{2+} + MnO_2 + H^+ \rightarrow MnOOH + Fe^{3+} \quad (8)$$

$$2Fe^{2+} + MnO_2 + 2H_2O \rightarrow Mn^{2+} + 2FeOOH + 2H^+ \quad (9)$$

Together with the reduction of the Mn species, the corroded Fe^{2+} (from the nZVI) was presumed to form oxyhydroxide products (MnOOH or FeOOH) contributing to the significant decrease in the iron released for the case of the nZVI/Mn oxide compared with that of the nZVI (Fig. 3b). On the other hand, the corroded Fe^{2+} in bare nZVI was primarily released into aqueous solution (Fu et al. 2014). These oxyhydroxide formations were able to provide active adsorption sites to subsequently adsorb/precipitate the dissolved iron species (Fe^{2+}/Fe^{3+}) (Btatkeu-K et al. 2014a; Noubactep 2010).

Moreover, this chemistry of the nZVI/Mn oxide was further supported by the HR-TEM image of the nZVI/Mn oxide after arsenic adsorption, which showed a single amorphous layer of mixed iron and manganese (hydr)oxides (refer to Fig. S2 in SI) from two separated layers of the shell in the fresh nZVI/Mn oxide (Fig. 1a). This means that the precipitates of the iron and manganese (hydr)oxides can be rearranged to form a single porous layer shell providing enlarged active adsorption sites which contribute to the

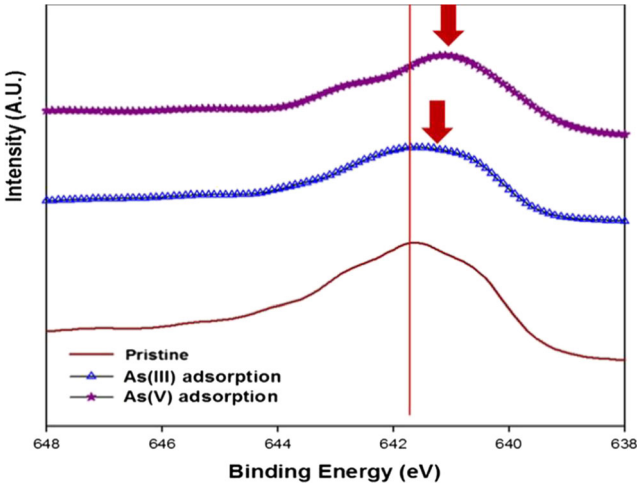

Fig. 4 XPS spectra (Mn 2*p*) of the nZVI/Mn oxide before and after adsorption of As(III) and As (V) ($[As(III)]_0 = [As(V)]_0 = 5$ mg L^{-1}, 0.3 g L^{-1} of the nZVI/Mn oxide)

improvement of the adsorption performance of both As(III) and As(V) compared with that of the nZVI (Zhang et al. 2009) (Table 1). This explanation is consistent with the higher adsorption capacity of the nZVI/Mn oxide compared to that of the nZVI in Fig. 2b. In addition, the increase in the surface area and pore volume (Table 1) supported that the Mn oxide can provide additional surfaces and pores that could partially enhance the arsenic adsorption capacity of the nZVI/Mn oxide. Furthermore, the Fe^{2+} capturing by the MnO_2 shell provided a favorable condition for the corrosion reaction of the Fe^0 core (Eq. (1)) by preventing iron (hydr)oxides from directly depositing onto the surface of the Fe^0 core. As a result, the reactivity of the nZVI/Mn oxide was sustained, and similar results have been reported in previous studies (Btatkeu-K et al. 2014a; Noubactep et al. 2011).

Conclusion

This study reports the development of an effective core/shell structural arsenic adsorbent comprised of nano zero-valent iron/manganese oxide (called the nZVI/Mn oxide). For arsenic removal, the nZVI/Mn oxide exhibited a great enhancement in its arsenic adsorption capacity (two and three times higher for As(III) and As(V), respectively) and long-term reusability for multiple cycles of regeneration compared with that of the nZVI. The chemistry behind the enhanced performance of the nZVI/Mn oxide for arsenic adsorption is explained by the synergistic activity between the nZVI core and the manganese oxide shell. Despite the better performance of the nZVI/Mn oxide for arsenic removal compared with that of the nZVI, further study is required to improve its suitability for application at near-to-neutral pH values.

Acknowledgements This research was supported by the R&D Program for the Society of the National Research Foundation (NRF) funded by the Ministry of Science, ICT & Future Planning (grant number NRF-2013K1A3A9A04043230) and by Korea Ministry of Environment as "Global Top Project (E617-00211-0608-0)", and a grant (code 17IFIP-B065893-05) from Industrial Facilities & Infrastructure Research Program funded by Ministry of Land, Infrastructure and Transport of Korean government.

References

Ahn S, Kang SM, Lee S-H, Park JB (2014) Facile synthesis of graphene-supported MnO, Mn_3O_4, and MnO_2 nanocomposites by controlling gas environment bull. Korean Chem Soc 35:2889–2890. https://doi.org/10.5012/bkcs.2014.35.10.2889

Asadullah M, Jahan I, Ahmed MB, Adawiyah P, Malek NH, Rahman MS (2014) Preparation of microporous activated carbon and its modification for arsenic removal from water. J Ind Eng Chem 20:887–896. https://doi.org/10.1016/j.jiec.2013.06.019

Bang S, Johnson MD, Korfiatis GP, Meng X (2005a) Chemical reactions between arsenic and zero-valent iron in water. Water Res 39:763–770. https://doi.org/10.1016/j.watres.2004.12.022

Bang S, Korfiatis GP, Meng X (2005b) Removal of arsenic from water by zero-valent iron. J Hazard Mater 121:61–67. https://doi.org/10.1016/j.jhazmat.2005.01.030

Bhowmick S et al (2014) Montmorillonite-supported nanoscale zero-valent iron for removal of arsenic from aqueous solution: kinetics and mechanism. Chem Eng J 243:14–23. https://doi.org/10.1016/j.Cej.2013.12.049

Bokare AD, Chikate RC, Rode CV, Paknikar KM (2008) Iron-nickel bimetallic nanoparticles for reductive degradation of azo dye Orange G in aqueous solution. Appl Catal B 79:270–278. https://doi.org/10.1016/j.Apcatb.2007.10.033

Btatkeu-K BD, Olvera-Vargas H, Tchatchueng JB, Noubactep C, Care S (2014a) Characterizing the impact of MnO_2 on the efficiency of Fe^0-based filtration systems. Chem Eng J 250:416–422. https://doi.org/10.1016/j.cej.2014.04.059

Btatkeu-K BD, Olvera-Vargas H, Tchatchueng JB, Noubactep C, Caré S (2014b) Determining the optimum Fe^0 ratio for sustainable granular Fe^0/sand water filters. Chem Eng J 247:265–274. https://doi.org/10.1016/j.Cej.2014.03.008

Chang YY, Lee SM, Yang JK (2009) Removal of As(III) and As(V) by natural and synthetic metal oxides colloids. Surf Physicochem Eng Asp 346:202–207. https://doi.org/10.1016/j.Colsurfa.2009.06.017

Choong TSY, Chuah TG, Robiah Y, Gregory Koay FL, Azni I (2007) Arsenic toxicity, health hazards and removal techniques from water: an overview. Desalination 217:139–166. https://doi.org/10.1016/j.desal.2007.01.015

Dharmarathna S, King'ondu CK, Pedrick W, Pahalagedara L, Suib SL (2012) Direct sonochemical synthesis of manganese octahedral molecular sieve (OMS-2) nanomaterials using cosolvent systems, their characterization, and catalytic applications. Chem Mater 24:705–712. https://doi.org/10.1021/cm203366m

Fu F, Dionysiou DD, Liu H (2014) The use of zero-valent iron for groundwater remediation and wastewater treatment: a review. J Hazard Mater 267:194–205. https://doi.org/10.1016/j.jhazmat.2013.12.062

Ghauch A, Abou Assi H, Bdeir S (2010a) Aqueous removal of diclofenac by plated elemental iron: bimetallic systems. J Hazard Mater 182:64–74. https://doi.org/10.1016/j.Jhazmat.2010.05.139

Ghauch A, Abou Assi H, Tuqan A (2010b) Investigating the mechanism of clofibric acid removal in Fe^0/H_2O systems. J Hazard Mater 176:48–55. https://doi.org/10.1016/j.jhazmat.2009.10.125

Grosvenor AP, Kobe BA, Biesinger MC, McIntyre NS (2004) Investigation of multiplet splitting of Fe 2p XPS spectra and

bonding in iron compounds. Surf Interface Anal 36:1564–1574. https://doi.org/10.1002/sia.1984

Gupta A, Chauhan VS, Sankararamakrishnan N (2009) Preparation and evaluation of iron–chitosan composites for removal of as(III) and as(V) from arsenic contaminated real life groundwater. Water Res 43:3862–3870. https://doi.org/10.1016/j.Watres.2009.05.040

Hristovski K, Baumgardner A, Westerhoff P (2007) Selecting metal oxide nanomaterials for arsenic removal in fixed bed columns: from nanopowders to aggregated nanoparticle media. J Hazard Mater 147:265–274. https://doi.org/10.1016/j.jhazmat.2007.01.017

Kanel SR, Manning B, Charlet L, Choi H (2005) Removal of arsenic(III) from groundwater by nanoscale zero-valent iron. Environ Sci Technol 39:1291–1298

Kawaoka H, Hibino M, Zhou H, Honma I (2005) Optimization of sonochemical synthesis condition of manganese oxide/acetylene black nanocomposite for high power lithium-ion batteries. J Electrochem Soc 152:A1217. https://doi.org/10.1149/1.1905965

Korngold E, Belayev N, Aronov L (2001) Removal of arsenic from drinking water by anion exchangers. Desalination 141:81–84. https://doi.org/10.1016/S0011-9164(01)00391-5

Mayo JT et al (2007) The effect of nanocrystalline magnetite size on arsenic removal. Sci Technol Adv Mater 8:71–75. https://doi.org/10.1016/j.stam.2006.10.005

Mohan D, Pittman CU Jr (2007) Arsenic removal from water/wastewater using adsorbents—a critical review. J Hazard Mater 142:1–53. https://doi.org/10.1016/j.jhazmat.2007.01.006

Nesbitt HW, Banerjee D (1998) Interpretation of XPS Mn(2p) spectra of Mn oxyhydroxides and constraints on the mechanism of MnO_2 precipitation. Am Mineral 83:305–315

Noubactep C (2010) The suitability of metallic iron for environmental remediation. Environ Prog Sustain Energy 29:286–291. https://doi.org/10.1002/ep.10406

Noubactep C, Btatkeu KBD, Tchatchueng JB (2011) Impact of MnO_2 on the efficiency of metallic iron for the removal of dissolved Cr^{VI}, Cu^{II}, Mo^{VI}, Sb^{V}, U^{VI} and Zn^{II}. Chem Eng J 178:78–84. https://doi.org/10.1016/j.cej.2011.10.014

Noubactep C, Caré S, Btatkeu KBD, Nanseu-Njiki CP (2012) Enhancing the sustainability of household Fe^0/sand filters by using Bimetallics and MnO_2. Clean: Soil, Air, Water 40:100–109. https://doi.org/10.1002/clen.201100014

Ramesh A, Hasegawa H, Maki T, Ueda K (2007) Adsorption of inorganic and organic arsenic from aqueous solutions by polymeric Al/Fe modified montmorillonite. Sep Purif Technol 56:90–100. https://doi.org/10.1016/j.Seppur.2007.01.025

Rivas BL, Del Carmen AM, Pereira E (2007) Cationic water-soluble polymers with the ability to remove arsenate through an ultrafiltration technique. J Appl Polym Sci 106:89–94

Sarkar S, Blaney LM, Gupta A, Ghosh D, SenGupta AK (2007) Use of ArsenXnp, a hybrid anion exchanger, for arsenic removal in remote villages in the Indian subcontinent. React Funct Polym 67:1599–1611. https://doi.org/10.1016/j.reactfunctpolym.2007.07.047

Sato N (1989) Toward a more fundamental understanding of corrosion processes. Corros Sci 45:354–368

Shan C, Tong M (2013) Efficient removal of trace arsenite through oxidation and adsorption by magnetic nanoparticles modified with Fe–Mn binary oxide. Water Res 47:3411–3421. https://doi.org/10.1016/j.Watres.2013.03.035

Singh R, Singh S, Parihar P, Singh VP, Prasad SM (2015) Arsenic contamination, consequences and remediation techniques: a review. Ecotoxicol Environ Saf 112:247–270. https://doi.org/10.1016/j.ecoenv.2014.10.009

Su C, Puls RW (2001a) Arsenate and arsenite removal by zerovalent iron: kinetics, redox transformation, and implications for in situ groundwater remediation. Environ Sci Technol 35:1487–1492

Su C, Puls RW (2001b) Arsenate and arsenite removal by zerovalent iron: effects of phosphate, silicate, carbonate, borate, sulfate, chromate, molybdate, and nitrate, relative to chloride. Environ Sci Technol 35:4562–4568. https://doi.org/10.1021/es010768z

Sun Y, Li X, Cao J, Zhang W, Wang HP (2006) Characterization of zero-valent iron nanoparticles. Adv Colloid Interface Sci 120:47–56. https://doi.org/10.1016/j.cis.2006.03.001

Tanboonchuy V, Hsu JC, Grisdanurak N, Liao CH (2011) Gas-bubbled nano zero-valent iron process for high concentration arsenate removal. J Hazard Mater 186:2123–2128. https://doi.org/10.1016/j.jhazmat.2010.12.125

Tang SCN, Lo IMC (2013) Magnetic nanoparticles: essential factors for sustainable environmental applications. Water Res 47:2613–2632. https://doi.org/10.1016/j.watres.2013.02.039

Wang C, Luo H, Zhang Z, Wu Y, Zhang J, Chen S (2014) Removal of As(III) and As(V) from aqueous solutions using nanoscale zero valent iron-reduced graphite oxide modified composites. J Hazard Mater 268:124–131. https://doi.org/10.1016/j.jhazmat.2014.01.009

Wen ZP, Zhang YL, Dai CM, Chen B, Guo SJ, Yu H, Wu DL (2014) Synthesis of ordered mesoporous iron manganese bimetal oxides for arsenic removal from aqueous solutions. Microporous Mesoporous Mater 200:235–244. https://doi.org/10.1016/j.micromeso.2014.08.049

Wu K, Liu T, Xue W, Wang XC (2012) Arsenic(III) oxidation/adsorption behaviors on a new bimetal adsorbent of Mn-oxide-doped Al oxide. Chem Eng J 192:343–349. https://doi.org/10.1016/j.cej.2012.03.058

Xi Y, Mallavarapu M, Naidu R (2010) Reduction and adsorption of Pb^{2+} in aqueous solution by nano-zero-valent iron–a SEM, TEM and XPS study. Mater Res Bull 45:1361–1367. https://doi.org/10.1016/j.materresbull.2010.06.046

Xu Y-h, Nakajima T, Ohki A (2002) Adsorption and removal of arsenic(V) from drinking water by aluminum-loaded Shirasu-zeolite. J Hazard Mater 92:275–287. https://doi.org/10.1016/S0304-3894(02)00020-1

Yamashita T, Hayes P (2008) Analysis of XPS spectra of Fe^{2+} and Fe^{3+} ions in oxide materials. Appl Surf Sci 254:2441–2449. https://doi.org/10.1016/j.apsusc.2007.09.063

Yang L, Wu SN, Chen JP (2007) Modification of activated carbon by polyaniline for enhanced adsorption of aqueous arsenate. Ind Eng Chem Res 46:2133–2140. https://doi.org/10.1021/ie0611352

Zhang X, Jiang K, Tian Z, Huang W, Zhao L (2008) Removal of arsenic in water by an ion-exchange fiber with amino groups. J Appl Polym Sci 110:3934–3940

Zhang G, Liu H, Liu R, Qu J (2009) Adsorption behavior and mechanism of arsenate at Fe–Mn binary oxide/water interface. J Hazard Mater 168:820–825. https://doi.org/10.1016/j.jhazmat.2009.02.137

Zhao Z, Liu J, Cui F, Feng H, Zhang L (2012) One pot synthesis of tunable Fe_3O_4–MnO_2 core–shell nanoplates and their applications for water purification. J Mater Chem 22:9052. https://doi.org/10.1039/c2jm00153e

Zhu H, Jia Y, Wu X, Wang H (2009) Removal of arsenic from water by supported nano zero-valent iron on activated carbon. J Hazard Mater 172:1591–1596. https://doi.org/10.1016/j.jhazmat.2009.08.031